

Speleothem record of geomagnetic South Atlantic Anomaly recurrence

Ricardo I. F. Trindade^{a,1,2}, Plinio Jaqueto^{a,2}, Filipe Terra-Nova^{a,b}, Daniele Brandt^a, Gelvam A. Hartmann^c, Joshua M. Feinberg^d, Becky E. Strauss^e, Valdir F. Novello^f, Francisco W. Cruz^f, Ivo Karmann^f, Hai Cheng^{g,h}, and R. Lawrence Edwards^g

^aInstituto de Astronomia, Geofísica e Ciências Atmosféricas, Universidade de São Paulo, 05508-090 São Paulo, Brazil; ^bLaboratoire de Planétologie et Géodynamique, Université de Nantes, F-44000 Nantes, France; 'Instituto de Geociências, Universidade Estadual de Campinas, 13083-870 Campinas, Brazil; ^dInstitute for Rock Magnetism, University of Minnesota, Minneapolis, MN 55455; ^eMaterial Measurement Laboratory, Materials Science and Engineering Division, National Institute of Standards and Technology, Gaithersburg, MD 20899; ^fInstituto de Geociências, Universidade de São Paulo, 05508-080 São Paulo, Brazil; ^gDepartment of Earth Sciences, University of Minnesota, Minneapolis, MN 55455; and ^hInstitute of Global Environmental Change, Xi'an Jiaotong University, 710049 Xi'an, China

Edited by Dennis V. Kent, Rutgers University, New Brunswick, NJ, and Lamont-Doherty Earth Observatory, Palisades, NY, and approved November 1, 2018 (received for review May 28, 2018)

The diminishing strength of the Earth's magnetic dipole over recent millennia is accompanied by the increasing prominence of the geomagnetic South Atlantic Anomaly (SAA), which spreads over the South Atlantic Ocean and South America. The longevity of this feature at millennial timescales is elusive because of the scarcity of continuous geomagnetic data for the region. Here, we report a unique geomagnetic record for the last \sim 1500 y that combines the data of two welldated stalagmites from Pau d'Alho cave, located close to the presentday minimum of the anomaly in central South America. Magnetic directions and relative paleointensity data for both stalagmites are generally consistent and agree with historical data from the last 500 y. Before 1500 CE, the data adhere to the geomagnetic model ARCH3K.1, which is derived solely from archeomagnetic data. Our observations indicate rapid directional variations (>0.1°/y) from approximately 860 to 960 CE and approximately 1450 to 1750 CE. A similar pattern of rapid directional variation observed from South Africa precedes the South American record by 224 \pm 50 y. These results confirm that fast geomagnetic field variations linked to the SAA are a recurrent feature in the region. We develop synthetic models of reversed magnetic flux patches at the core-mantle boundary and calculate their expression at the Earth's surface. The models that qualitatively resemble the observational data involve westward (and southward) migration of midlatitude patches, combined with their expansion and intensification.

archeomagnetism | South Atlantic Anomaly | speleothem | geomagnetism | paleomagnetism

he South Atlantic Anomaly (SAA) marks the position of the weakest geomagnetic field on Earth, and has long been recognized as a major sink for high-energy particles in the magnetosphere, with consequences for orbiting satellites, as well as telecommunication networks and transmission grids (1). Historical geomagnetic data from ship logs, magnetic observatories, and, more recently, from satellites indicate that the SAA has been a prominent feature of the geomagnetic field since at least 1590 CE (2-4). These records indicate that the size of the anomaly has increased concomitant with increasing prominence (i.e., ever-weakening field intensity), and the anomaly has migrated continuously westward at a mean longitudinal speed of 0.17° y⁻¹. Areal growth and intensity decay are linked to the first-order variations of the geomagnetic field, more specifically, the relative increase of nondipole terms relative to the overall field geometry (2, 5) and the steady decay in the dipole moment itself at a rate of $\sim 15 \text{ nT y}^{-1}$ (4, 6). These effects reflect deep Earth processes emanating from the core–mantle boundary (CMB), where the proliferation of reverse flux patches (RFPs), particularly beneath the South Atlantic, causes a breakdown in symmetry in the advection sources of the axial dipole moment (4, 7).

Reconstructing the SAA anomaly at the so-called archeomagnetic (or millennial) timescale is not trivial, mainly due to the scarcity of geomagnetic data in the Southern Hemisphere (8, 9). Besides recent advances in data acquisition (10–13), the archeomagnetic

datasets from Africa and South America that are essential for the reconstruction of the SAA evolution contribute respectively only 2.5% and 2.8% to the global geomagnetic database (9). Directional and intensity data recently obtained for Africa indicate relatively rapid directional changes (>0.1° y⁻¹) between approximately 400 to 550 CE, approximately 550 to 750 CE, and approximately 1225 to 1550 CE accompanied by a fast decrease in intensity of -54 ± 36 nT y⁻¹ (10, 11). In comparison, a recent assessment of the archeomagnetic database for South America revealed only two intensity values before 1500 CE (13). Most archeomagnetic data from South America are limited to historical lava flows and baked-clay artifacts produced after the arrival of Europeans at 1500 CE. Several attempts to obtain archeomagnetic data from pre-Columbian archeological artifacts in Brazil and neighboring countries have been unsuccessful, mostly due to the incomplete baking of native ceramics (14). As a consequence, the only records of the geomagnetic field for South America at the millennial

Significance

Experimental and modeling evidence demonstrate the recurrence of the South Atlantic Anomaly. The areal growth of this geomagnetic anomaly accompanies the fast decay of the Earth's magnetic field, but its origin and longevity are still poorly understood given the scarcity of geomagnetic data in the Southern Hemisphere. We report a ~1500-y record with unprecedented resolution obtained close to the present-day minimum of the anomaly in South America from continuously grown cave speleothems. This unique record reveals rapid variations in direction and intensity of the local field as a function of the location and magnitude of the anomaly. Synthetic secular variation models show this feature may result from westward migration, expansion, and intensification of reversed flux patches on the coremantle boundary.

Author contributions: R.I.F.T., P.J., F.W.C., and I.K. designed research; R.I.F.T., P.J., F.T.-N., D.B., G.A.H., J.M.F., B.E.S., V.F.N., F.W.C., I.K., H.C., and R.L.E. performed research; P.J. and V.F.N. collected the samples; V.F.N., H.C., and R.L.E. dated the stalagmites; R.I.F.T., P.J., D.B., and G.A.H. performed paleomagnetic analysis and interpretation; P.J., J.M.F., and B.E.S. performed rock magnetic experiments; F.T.-N. produced synthetic secular variation scenarios; and R.I.F.T., P.J., and F.T.-N. wrote the paper with assistance from all authors.

The authors declare no conflict of interest.

This article is a PNAS Direct Submission.

Published under the PNAS license.

Data deposition: All data have been deposited in Earthref.org, https://earthref.org/MagIC/16523/8066c18d-ac66-470c-a3d6-2368f3c90bc5.

See Commentary on page 13154.

¹To whom correspondence should be addressed. Email: ricardo.trindade@iag.usp.br.

²R.I.F.T. and P.J. contributed equally to this work.

This article contains supporting information online at www.pnas.org/lookup/suppl/doi:10.1073/pnas.1809197115/-/DCSupplemental.

Published online December 10, 2018.

timescale are provided from studies of lake sediments [e.g., Escondido Lake (15)].

Baked-clay archeological artifacts and sediments are the classical archives used to reconstruct the archeomagnetic field. However, each of these records comes with caveats, particularly in recovering the Earth's field fluctuations at the centennial to millennial timescales. Baked-clay archeological artifacts (and lavas) provide an absolute measure of the field intensity based on thermoremanent magnetization (16), but these materials provide only episodic snapshots of the field. Sediments have the advantage of providing a continuous directional record of the local geomagnetic direction, but age uncertainties from sediments are typically on the order of hundreds to thousands years (17, 18). Sedimentary paleomagnetic records can also be afflicted by a delay between the age of sedimentation and the age of magnetization (19, 20) or be obliterated by further diagenesis (21). In addition, sediments can be affected by dewatering and compaction after remanence acquisition (22, 23), which produces shallower magnetic vectors. Speleothems, on the other hand, present several advantages over archeomagnetic and sedimentary archives by being usually continuous over thousands of years and readily dated at a very high precision by the radiometric ²³⁴U-²³⁰Th method (half-life of 245,000 y). As chemical precipitates, speleothems are not affected by postdepositional compaction effects (24). Moreover, in contrast to soft sediments, the time lag between deposition of magnetic particles on the top of the stalagmite and remanence lock-in is very short, comprising hundreds of seconds at most (24, 25), therefore ideally allowing the radiometric age obtained for each layer to be directly attributed to the remanence recorded in it.

Here, we provide a \sim 1,500-y geomagnetic field record for central South America based on the magnetic remanence of two rapidly grown and well-dated stalagmites. This high-resolution record reveals periods of rapid changes in the direction and intensity of the field out-of-phase with similar events in Africa (11). Then, synthetic models of migration, expansion, and intensification of reversed magnetic flux patches are applied to test the mechanisms at the origin of the observed field variations.

Sampling and Dating of Pau d'Alho Stalagmites

Paleomagnetic and relative paleointensity data were obtained from two stalagmites from the Pau d'Alho cave system (15°12'20" S, 56°48′41″ W), which is located near the present-day minimum of the SAA, in Midwest Brazil. Samples Alho 06 and Alho 31 are cylindrical stalagmites, respectively 240 and 135 mm tall, with a nearly constant diameter of ~6 cm (Fig. 1). The dominant mineralogy, determined by X-ray diffraction in both samples, is magnesian calcite (~97%) with minor amounts of dolomite and quartz attributed to the detrital contribution from weathered dolomitic host rock. The internal structure is marked by a very regular stratigraphy of alternated millimetric layers of light-gray to brownish calcite, with no evidence of hiatuses. Different strategies were used for their azimuthal orientation. Alho 31 was oriented in situ with a magnetic compass, and its declination was rotated by the azimuth measured during sampling, whereas Alho 06 had its declination rotated to the average declination of the International Geomagnetic Reference Field model (-3.68°) for the age of the youngest specimen (1932 CE \pm 23 y). The speleothem samples were cut into specimens consisting of thin slices of \sim 7 mm (Alho 06: 34 specimens) and \sim 5 mm (Alho 31: 27 specimens). U-Th dating shows mean growth rates of 0.169 ± 0.004 mm y⁻¹ (543 to 1932 CE) for Alho 06 (26) and 0.151 ± 0.008 mm y⁻¹ (1090 to 1922 CE) for Alho 31 (Fig. 1 and SI Appendix, Table \$1). These relatively high growth rates imply that each 7- or 5-mm specimen records a few decades of the geomagnetic field (~39 y for Alho 06 and ~32 y for Alho 31). Changes in growth rate are observed in both stalagmites, most pronouncedly at 30–50 mm from the top for Alho 06 and 40–75 mm from the top for Alho 31. The conversion of depth to age follows the model of Fig. 1 and therefore takes these changes into account. The most significant increase in accumulation rates observed in the two studied stalagmites occur in the interval between 1600 and 1820 CE, when precipitation was higher in the region throughout the Little Ice

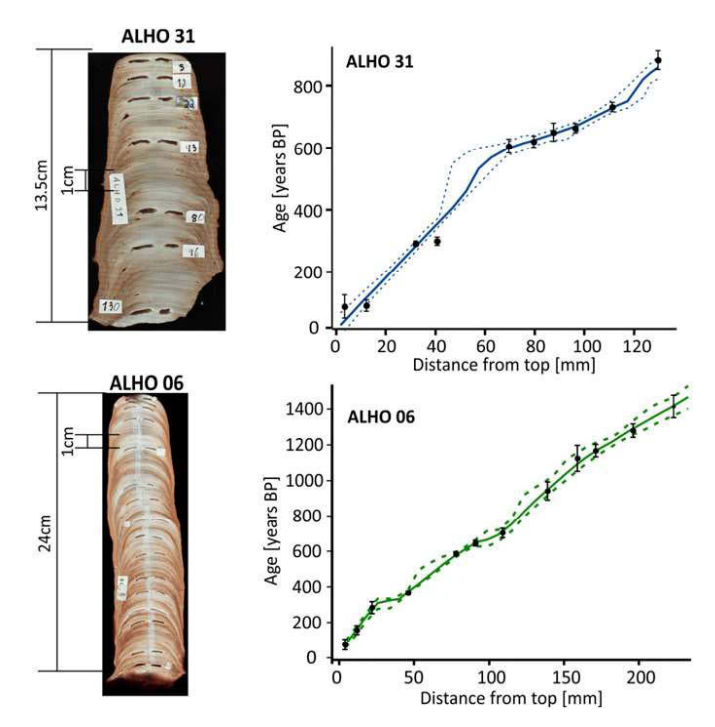


Fig. 1. Stalagmites from Pau d'Alho cave (15°12′20″S, 56°48′41″W). Samples Alho 31 (*Upper*) and Alho 06 (*Lower*) with respective U-Th dating points and age model are shown. Dashed lines indicate 95% confidence (2 σ) calculated from Monte Carlo fitting of ensembles of straight lines.

Age period (26). Both stalagmites ceased growth at the beginning of the last century, probably also due to changes in the hydrology of the cave resulting either from a dry period or by the blocking, in the epikarst, of the drip water supply to the speleothems.

Origin and Identification of Magnetic Minerals

The main magnetic mineral in both stalagmites is magnetite. Lowtemperature experiments on bulk samples show a Verwey transition (~120 K) in room-temperature saturation isothermal remanent curves (SI Appendix, Fig. S1). This transition is accentuated when analyzing the magnetic separates from the same samples (SI Appendix, Fig. S2). Goethite is also found, being identified by the characteristic separation of field cooling and zero-field cooling curves in the separates (SI Appendix, Fig. S2). The origin of magnetite can be inferred from coercivity unmixing analyses of anhysteretic remanent magnetization (ARM) curves (SI Appendix, Fig. S3) (27). ARM data in all previous studies of speleothems plot in the field of extracellular and pedogenic magnetite (28), including stalagmites from Spain (29), Portugal (30), South China (31), Brazil (32), and different sectors of the United States (24, 33) (SI Appendix, Fig. S4). In the Pau d'Alho cave, the magnetic mineralogy of soils above the cave was compared with the magnetic minerals present in the stalagmite (32). Their similarity further reinforces a pedogenic origin for the magnetic particles deposited in the stalagmite, likely formed through dissimilatory iron reduction in the soil (e.g., refs. 32) and 33). Type and size of magnetic minerals throughout the speleothems vary little and typically present, respectively for Alho 06 and Alho 31, median destructive fields of ~16 and ~13 mT and dispersion parameters of ~0.29 and ~0.27 (SI Appendix, Fig. S2). First-order reversal curves (FORCs) for Alho 06 and Alho 31 indicate that magnetite grains are in the single-domain range without significant magnetic interaction (SI Appendix, Fig. S5).

Paleomagnetic Directions and Paleointensity

Detailed stepwise alternating field (AF) demagnetization of all specimens was performed in a superconducting rock magnetometer, followed by principal component analysis. Specimens' volumes vary from 1.08 to 2.61 cm³ (mean of 1.79 cm³). Initial

magnetic moment of Alho 06 and Alho 31 are, on average, 2.8×10^{-9} and 2.3×10^{-9} A m², respectively. The relatively high initial magnetization enabled useful directional data on a resolution of tens of years per specimen to be obtained in a commercial cryogenic magnetometer, which, in our case, has a practical sensitivity higher than 6×10^{-11} A m² (SI Appendix, Fig. S6). Vector directions were calculated with an AF range between 12 and 35 mT, which corresponds to 12-54% of the NRM (Fig. 2). A magnetic remanence (<10%) that persisted above an applied field of 120 mT is associated with goethite (Fig. 2). Five specimens out of 61 displayed unstable behavior during demagnetization or maximum angular deviation (MAD) $\geq 20^{\circ}$, and these specimens are not further discussed.

The two stalagmites record deposition between approximately 1100 CE and approximately 1920 CE. Almost all magnetic declinations agree within error for this time period, whereas the magnetic inclinations show a ~10° difference between stalagmites (Fig. 3 and SI Appendix, Table S2). One possibility to account for this systematic difference is the rolling of magnetic particles at the border of the stalagmite (34). Magnetic grains in Alho 06 are arranged along an inclined plane as depicted from anisotropy of remanence measurements (SI Appendix, Fig. S7), suggesting that its specimens comprise the sloping border of the stalagmite. In contrast, magnetic grains in Alho 31 specimens (SI Appendix, Fig. S7) are arranged along the horizontal plane being thus immune to these effects. Other possibility would be a different degree of compaction between the stalagmites, but the average anisotropy degrees for Alho 06 and Alho 31 are 1.035 and 1.040, respectively, which imply similar compaction corrections of less than 2° for both stalagmites (35).

The Alho 06 record covers a longer period of time starting at ~543 CE. Taking the entire record, magnetic declinations starting from 543 CE show two cycles of changing declination, with positive peaks at approximately 900 CE and approximately 1700 CE, and a negative peak at ~1200 CE. Declination has been decreasing since ~1700 CE. The magnetic inclination for the same stalagmite increases from approximately 543 CE until approximately 1100 CE, followed by a progressive decrease from about -40° to near 0° in recent times.

In addition to the directional data, the relative paleointensity was estimated for all specimens that presented MAD values lower than 20°. Paleointensity estimations using the pseudo-Thellier method (36) were made across the same alternating field range used in the vectorial analysis (Fig. 2). We retained only specimens whose SE of the slope is less than 5% and the NRM fraction used in pseudo-Arai plots exceeds 25% (SI Appendix, Table S2). The well-defined, straight pseudo-Arai plots obtained from our specimens corroborate the single-domain nature of the magnetic assemblage inferred from FORC curves, whereas curved pseudo-Arai diagrams would indicate the presence multidomain grains (36). There is a considerable variability of relative intensity estimates in these weakly magnetic rocks, particularly in the interval of 1200 to 1400 CE for Alho 31 and at around 1600 CE for Alho 06. Notwithstanding, a general trend of geomagnetic field evolution for the past millennium is reproduced in the two stalagmites (Fig. 3). The two curves also overlap the general pattern defined by the high quality archeointensity data for South America (13), with marked intensity peaks at approximately 900 CE and approximately 1450 CE observed against a backdrop of decreasing field strength (Fig. 3).

Stalagmite Record vs. Geomagnetic Field Models

Previous use of speleothems as recorders of the geomagnetic field has been focused on long-term variations or magnetic excursion events (24, 29). Here, we show that two well-dated, fastgrown stalagmites reproduce the field within error at a ~40-v resolution for the last 1500 y (Fig. 3). The speleothem record matches both in direction and intensity the evolution of the field described by the geomagnetic models for recent times, when historical records are used to constrain the models HFM.OL1. A1, CALS3k.4e, and ARCH3k.1 (Fig. 3). Before 1200 CE, the models diverge, most likely due to the different datasets on which they are based on (17, 18). It is noteworthy that field direction and intensity retrieved from the stalagmite data follow the ARCH3k.1 model (17), which was constructed solely from archeomagnetic data with no input from South America. Archeomagnetic data from South America for the interval of 800 to 1200 CE obtained after the model was made are plotted in Fig. 3 and corroborate the ARCH3k.1 model. In contrast, the other models (HFM.OL1.A1 and CALS3k.4e) include lake sediment data from Argentina that typically drive the model to lower intensities in the interval of 400 to 1000 CE, a pattern that is not reproduced in our stalagmite data.

Rapid Directional Changes in South America and South Africa

A combined curve of paleosecular variation was constructed for the two stalagmites (Fig. 4A and SI Appendix, Table S3). This curve traces a coherent loop that matches the ARCH3k.1 model within error for the Pau d'Alho location. The data describe a clockwise loop from approximately 570 CE to approximately 1450 CE, followed by a northward departure up to approximately 1700 CE and then a rapid westward migration until approximately 1920 CE. The validity of the stalagmite results is reinforced by the good match of the angular variation recorded in this archive compared with that of the geomagnetic model from the period between 1590 and 1900 CE

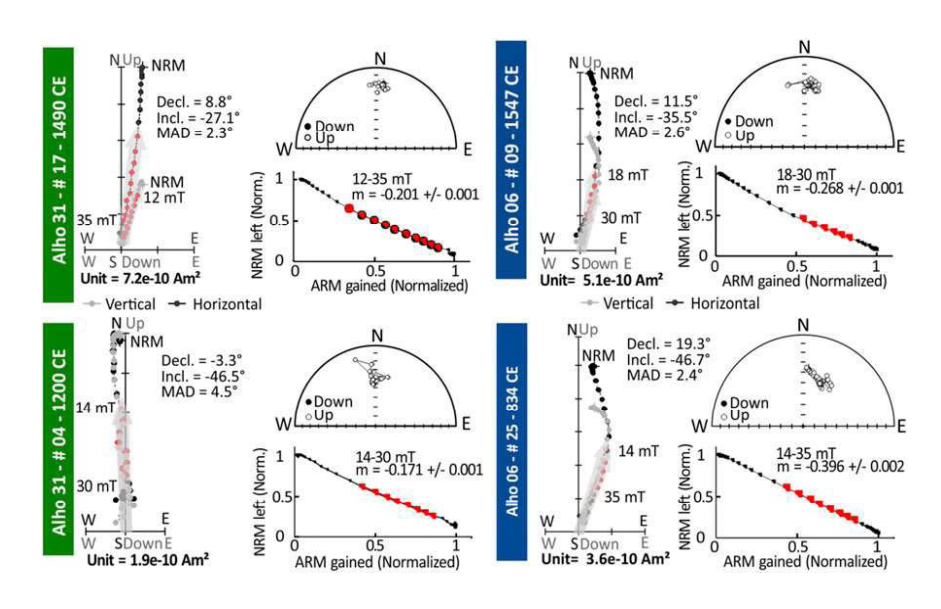


Fig. 2. Examples of magnetic directions and relative paleointensities. Shown are orthogonal vector plots and stereographic projections of alternating field demagnetization data and respective relative paleointensity estimates for two specimens from each stalagmite (ages and specimen numbers are indicated) Declination and inclination of magnetic vectors (gray arrows) obtained with principal component analysis (AF range in red) are given, together with their respective MAD. Relative paleointensity was estimated following the pseudo-Thellier method (36), with m representing the slope of the curve ARM gained-NRM left-Errors in m correspond to 2 σ .

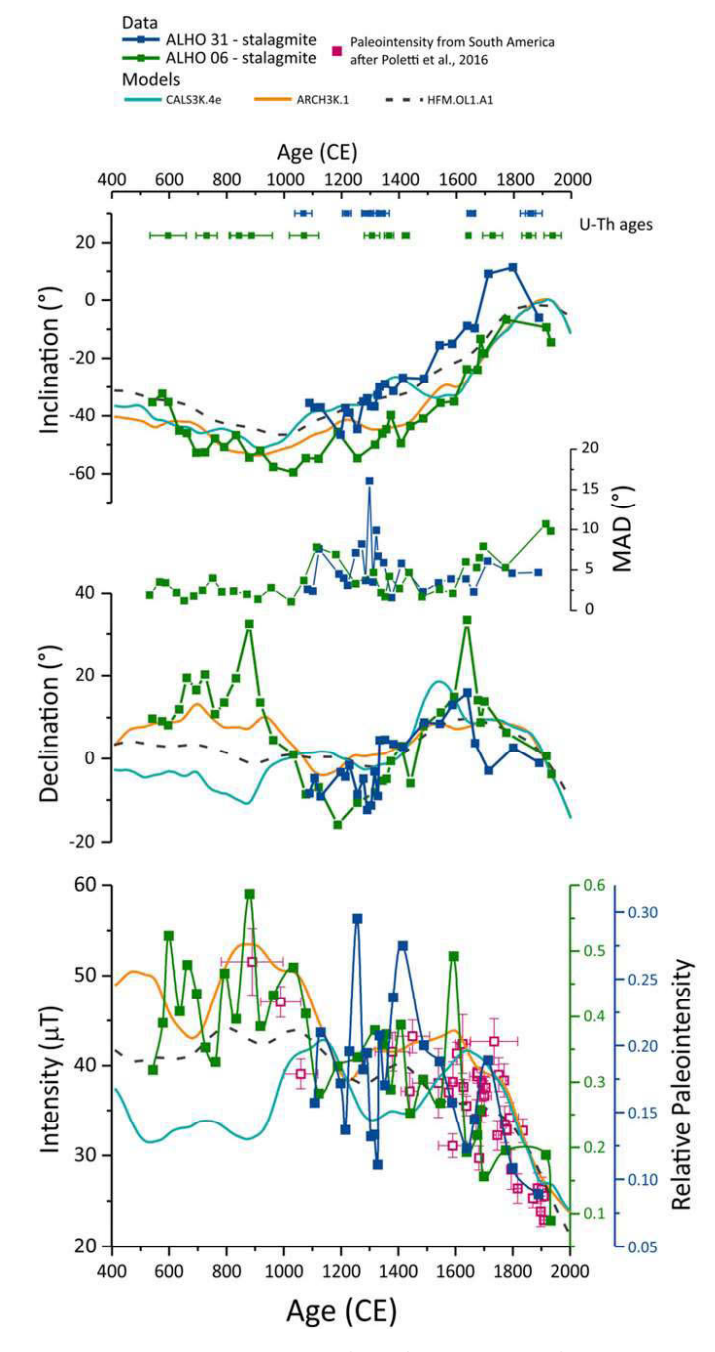


Fig. 3. Continuous magnetic results and comparison with geomagnetic models. Shown are radiometric ages (U-Th), magnetic declination, MAD, magnetic inclination, and relative paleointensity for specimens from Alho 31 (dark green) and Alho 06 (dark blue). Paleomagnetic results are compared with global geomagnetic field models for the Pau D'Alho cave location. CAL53k.4e (light blue) stands for "Continuous model from Archeomagnetic and Lake Sediment data" for the last 3 ka (17). Model ARCH3k.1 (orange) stands for "Archeomagnetic data" for the last 3 ka (17). Model HFM.OL1.A1 stands for "Holocene Field Model" (18). This last model accounts for archaeomagnetic, lava flows, and sedimentary data covering the past 10 ka and is less sensitive to outliers than CAL53k.4e yielding more stable estimates. From 1840 to 1990 CE, the three geomagnetic models are constrained by the *gufm1* model (6). Also shown are the high-quality South American archeointensity data from bricks, ceramics, tile, and historic basalts for the last 700 y (pink squares and error bars); these data were relocated to the Pau d'Alho location for comparison (13).

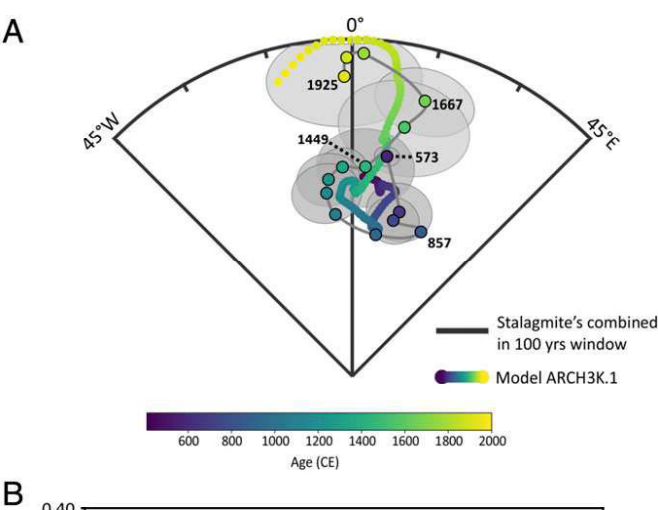
(Fig. 4*B*), where the ARCH3k.1 model is constrained by the historical records (6, 17). Starting from 570 CE, the variation observed on the stalagmite record is \sim 0.10° y⁻¹ until approximately 1450 CE,

with a peak of 0.12° y⁻¹ at approximately 900 CE. After 1450 CE, there is a general increase, with marked shifts at approximately 1500 CE and 1700 CE.

The angular variation of Pau d'Alho stalagmites can be compared with that obtained from archeological burnt clay structures in South Africa (11). A meaningful coherence between them is observed from 1225 CE (South Africa) to 1449 CE (South America), where both paths increase their angular variation to $\sim 0.13^{\circ} \text{ y}^{-1}$ (Fig. 4B) with a time lag of 224 ± 50 y. This result is validated by the ARCH3k.1 model in their respective locations for this period. Between approximately 1200 CE and approximately 600 CE, the same trends are observed in stalagmite and burnt clay structures, with a decrease in South Africa from approximately 550 CE to approximately 750 CE and a similar decrease in South America from approximately 850 CE to approximately 1150 CE. Interestingly, the increase in directional changes recorded in Pau d'Alho stalagmites is accompanied by a decay in intensity values in the ARCH3k.1 model; this is observed at approximately 900 CE and at approximately 1450 CE. These rapid changes in paleointensity were found in South Africa (11), again with a time lag of ~200 y between Africa and South America for the last period.

A Recurrent South Atlantic Anomaly?

The SAA may be a very ancient feature of the geomagnetic field. According to Tarduno et al. (10), a large and long-lived mantle



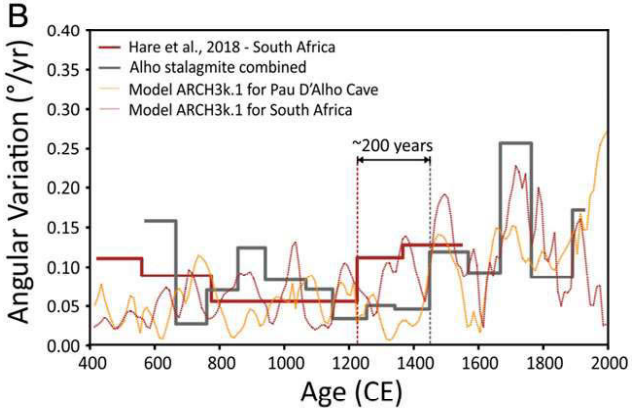


Fig. 4. Geomagnetic SV. (A) Stereonet of 100-y, window-combined stalagmite directional data with 95% confidence ellipses (2 σ) with respective mean ages and comparison with model ARCH3k.1 (45); the color scale corresponds to age. (*B*) Angular variation of the field from South America (gray line) and South Africa (dark-red line) (11); the orange dashed line represents the model ARCH3k.1 for Pau d'Alho location, and the dark-brown dashed line represents model ARCH3k.1 for the center of South Africa (11). Errors correspond to 63% confidence levels (1 σ) as in ref. 11. Red (gray) bars indicate intervals with rapid directional variation in the geomagnetic field in Africa (South America).

heterogeneity stationed beneath Africa would control the preferential location of RFPs at the CMB by inducing local topographic roughness at the CMB making this region a preferential site for flux expulsion from the core. The RFPs originated in Africa would then drift westward, toward South America. The tracking of RFPs throughout the last 3000 y using the available geomagnetic field models attests to the recurrence of reverse patches at specific regions and supports the hypothesis that links them to mantle heterogeneities (37), but when kernel functions that link the location of reverse patches at depth to the location of the anomalies at the planet's surface are considered, a straightforward link between these features and the SAA has not been be established (38).

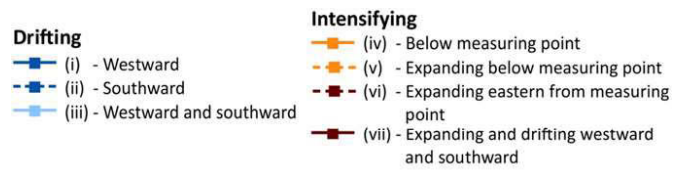
To test the mechanisms that would potentially contribute to the rapid field changes observed in South America and South Africa and the delay between records at each side of the South Atlantic, we conducted a series of seven synthetic tests of secular variation (SV) (Fig. 5 and SI Appendix, Table S4) over a 400 y timespan. In these tests, advection is given by westward and southward drift, stretching is represented by expansion of RFPs and diffusion by their intensification (see details in SI Appendix and in SI Appendix, Table S4).

Changes in field direction and strength observed at centennial scale for both continents are not reproduced by a single mechanism (Fig. 5). Westward drift of an RFP (Fig. 5, scenario i) is the most efficient of the tested mechanisms for rapid changes of declination but cannot account for the observed changes in inclination and field strength. The combination of expansion and intensification of an RFP is more effective in changing inclination than westward drift, but this scenario is more efficient when the RFP grows eastwards than just below the measuring point. Field intensity decreases in all tested SV scenarios, but those involving exclusively advection of an RFP were the least efficient. Intensification works better when coupled with expansion and when the RFP is not below the measuring point. Finally, when all SV mechanisms are combined the directional and intensity changes are the most pronounced. Of the scenarios considered, this is the only one where rapid intensity decay and sharp directional changes occur and are shifted in time, mirroring the observation (Fig. 5 and SI Appendix, Table S4). Usually, the fastest intensity decay can be thought as the result of the arrival of the anomaly and the rapid changes in declination correspond to when the center of the anomaly is the closest to the measuring point.

The synthetic scenarios are simple approximations of the field and lack the complexity of the Earth's actual magnetic field. However, these models do give insights into how an RFP can alter the geomagnetic record and what to expect in a measuring point where an RFP region is prominent as over the South Atlantic Ocean. In our analysis, westward drift is by far the main source of observed sharp changes in declination, but as previously suggested (10, 11), intensification and expansion of RFPs are also needed to produce the abrupt variations of inclination and the rapid decay of intensity observed. Moreover, in a scenario where changes in inclination are more pronounced than in declination the SV needs more than a zonal source of field drift. Our results suggest that upwelling structures and diffusion were present at least as early as ~1450 CE in the South Atlantic region, and possibly as early as ~860 CE. Therefore, a weak-field anomaly at the South Atlantic is expected to be recurrent as previously suggested (10, 11). Finally, the time lag of ~200 y between the rapid intensity decays in Africa and South America is too short for a pure advective scenario of RFPs migrating from Africa to South America, suggesting that flux expulsion in South America may also contribute to the SAA time evolution.

Materials and Methods

U-Th Dating. Radiometric dating was carried out at the Minnesota Isotope Laboratory using a multicollector inductive plasma mass spectrometer [NEPTUNE (Thermo-Finnigan)] (39). Ten new U-Th ages were obtained for Alho 31 sample (*SI Appendix*, Table S1). Ages for Alho 06 were compiled from Novello et al. (26). Age models and corresponding 95% confidence limits were obtained through Monte Carlo fitting of ensembles of straight lines with the software StalAge (40).



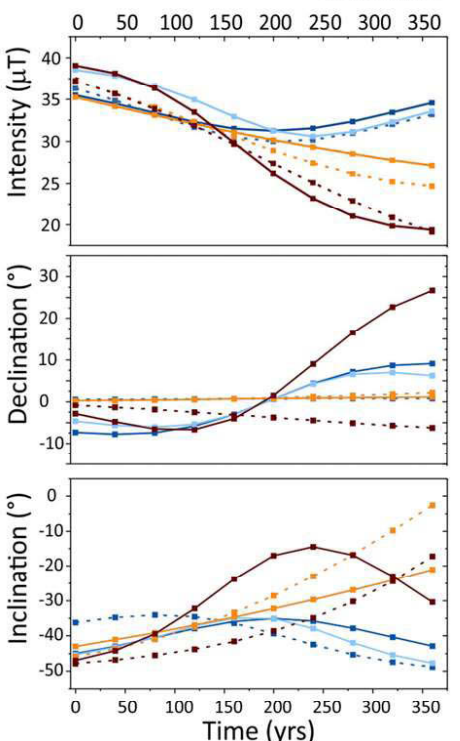


Fig. 5. Secular variation scenarios. Dark-blue solid lines indicate westward drift (*i*), dark-blue dashed lines indicate southward drift (*ii*), light-blue solid lines indicate westward coupled with southward drift (iii), orange solid lines indicate intensification (*iv*), orange dashed lines indicate intensification and expansion (*v*), brown dashed lines indicate eastern intensification and expansion (*vi*), and brown solid lines indicate all SV mechanisms (*vii*). Note that for westward drift (dark-blue solid line curve), there is a mirror effect, whereas for SV scenarios with southward drift, a faster decay is observed as RFP approaches and slower enhancing is observed as it goes away. These effects are not seen when all SV mechanisms are applied due to their large influence time (brown solid lines).

Paleomagnetism and Paleointensity. Measurements were carried out at Laboratório de Paleomagnetismo of Universidade de São Paulo. Remanence was measured in a 755-1.65 2G Enterprises DC SQUID magnetometer (practical sensitivity better than 6×10^{-11} A m⁻²; *SI Appendix*, Fig. S6) housed in a shielded room with ambient field <200 nT. Specimens were submitted to stepwise AF demagnetization along 30 steps up to 140 mT. Directions were analyzed using principal component analysis (41). Relative paleointensity estimates followed the pseudo-Thellier method (40). Specimens were submitted to a direct field of 0.05 mT along the same AF steps used in the AF demagnetization. The slope of the ARM $_{\rm gained}$ -NRM $_{\rm left}$ curve was calculated using the line fitting method of refs. 16 and 36.

Magnetic Mineralogy. ARM acquisition was performed on bulk Pau d'Alho samples with a direct field of 0.05 mT along 33 steps of alternating field up to 120 mT and analyzed with MAXUNMIX software (27). FORCs were done in a Princeton Measurements Corporation vibrating sample magnetometer using a variable resolution that enables high-resolution analysis (42) after adjustment of hysteresis curves with XFORC software (43). Magnetic extraction with an Nd magnet was then performed to concentrate ferromagnetic material and remove the masking effect of the diamagnetic calcite matrix (44). Room-temperature saturation isothermal remanent magnetization and field cooling–zero-field cooling experiments on magnetic extracts were performed using a Quantum Designs Magnetic

Properties Measurement System (MPMS-5S) in the Institute for Rock Magnetism (IRM) at the University of Minnesota.

Geomagnetic Angular Variation. The directional variation of the geomagnetic record was evaluated using data from both stalagmites combined in a running mean with 100 y of interval (45). The angular rate was calculated by the ratio of the angular distance between each point of the path and the corresponding interval of time. The error of angular rate was calculated using the propagation of the 63% of confidence angle (α_{63}) as the angular error for each mean and the SD of the ages from the grouped directions (11) (SI Appendix, Table S3).

Synthetic Models. Synthetic tests were performed for simple radial field configurations at the CMB and their effects on the Earth's surface using appropriate kernel functions (38) (see details in SI Appendix). The synthetic fields were built from a background axial dipole field superimposed by local patches modeled by gaussians (38). Fluxes were set to maintain $\int_{S} B_r dS = 0$. In our synthetic SV scenarios, advection is given by westward and southward drift, stretching by expansion and diffusion by intensification of RFPs. Westward drift value used was the classical one of 0.2° y⁻¹ (46). Southward drift

- 1. Heirtzler JR (2002) The future of the South Atlantic anomaly and implications for radiation damage in space. J Atmos Sol Terr Phys 64:1701-1708
- 2. Hartmann GA, Pacca IG (2009) Time evolution of the South Atlantic magnetic anomaly. An Acad Bras Cienc 81:243-255.
- 3. Thébault E, Finlay CC, Toh H (2015) International geomagnetic reference field: The 12th generation. Earth Planet Space 67:158.
- 4. Finlay CC, Aubert J, Gillet N (2016) Gyre-driven decay of the earth's magnetic dipole. Nat Commun 7:10422.
- 5. Pavon-Carrasco FJ, De Santis A (2016) The South Atlantic anomaly: The key for a possible geomagnetic reversal. Front Earth Sci 4:1-9.
- Jackson A, Jonkers ART, Walker MR (2000) Four centuries of geomagnetic secular variation from historical records. Philos Trans R Soc A 358:957-990.
- Gubbins D, Jones AL, Finlay CC (2006) Fall in earth's magnetic field is erratic. Science 312:900-902.
- Donadini F, Korte M, Constable CG (2009) Geomagnetic field for 0-3 ka: 1. New data sets for global modeling. Geochem Geophys Geosyst 10:Q06008.
- 9. Brown MC, et al. (2015) GEOMAGIA50.v3: 2. A new paleomagnetic database for lake and marine sediments. Earth Planets Space 67:83.
- Tarduno JA, et al. (2015) Antiquity of the South Atlantic anomaly and evidence for top-down control on the geodynamo. Nat Commun 6:7865.
- 11. Hare VJ, et al. (2018) New archeomagnetic directional records from iron age Southern Africa (ca. 425-1550 CE) and implications for the South Atlantic anomaly. Geophys Res Lett 45:1361-1369
- 12. Roperch P, Chauvin A, Lara LE, Moreno H (2015) Secular variation of the earth's magnetic field and application to paleomagnetic dating of historical lava flows in Chile. Phys Earth Planet Inter 242:65-78.
- 13. Poletti W. Trindade RIF. Hartmann GA. Damiani N. Rech RM (2016) Archeomagnetism of Jesuit missions in South Brazil (1657-1706 AD) and assessment of the South American database. Earth Planet Sci Lett 445:36-47.
- 14. Hartmann GA, Afonso MC, Trindade RIF (2011) Preliminary results of magnetic archaeointensity measurements in Brazil. Proceedings of the 37th International Symposium on Archaeometry, ed Turbanti-Memmi I (Springer, Berlin), pp 495-499.
- 15. Gogorza CSG, et al. (2004) Paleointensity studies on Holocene-Pleistocene sediments from Lake Escondido, Argentina. Phys Earth Planet Inter 145:219-238.
- 16. Coe RS (1967) Determination of paleo-intensities of earths magnetic field with emphasis on mechanisms which could cause non-ideal behavior in Thelliers method. J Geomag Geoelectr 19:157–179.
- 17. Korte M, Constable C (2011) Improving geomagnetic field reconstructions for 0–3ka. Phys Earth Planet Inter 188:247-259.
- Panovska S, Korte M, Finlay CC, Constable CG (2015) Limitations in paleomagnetic data and modelling techniques and their impact on Holocene geomagnetic field models. Geophys J Int 202:402-418.
- 19. Tauxe L, Steindorf JL, Harris A (2006) Depositional remanent magnetization: Toward an improved theoretical and experimental foundation. Earth Planet Sci Lett 244:515-529.
- 20. Nilsson A, Holme R, Korte M, Suttie N, Hill M (2014) Reconstructing Holocene geomagnetic field variation: New methods, models and implications. Geophys J Int 198:229-248.
- 21. Roberts AP (2015) Magnetic mineral diagenesis. Earth Sci Rev 151:1-47.
- 22. Lascu I, Feinberg JM (2011) Speleothem magnetism. Quat Sci Rev 30:3306-3320.
- 23. Tauxe L, Kent DV (2004) A simplified statistical model for the geomagnetic field and the detection of shallow bias in paleomagnetic inclinations: Was the ancient magnetic field dipolar? Geophys Monogr Ser 145:101-115
- 24. Lascu I, Feinberg JM, Dorale JA, Cheng H, Edwards RL (2016) Age of the Laschamp excursion determined by U-Th dating of a speleothem geomagnetic record from North America. Geology 44:139-142.

is 0.15° y⁻¹ based on the evolution of the Patagonia RFP from 1930 until 1970 CE in the geomagnetic model gufm1 (6, 38). Intensification is based on values of reversed flux intensification on the Southern Hemisphere during the historical period (47). Expansion scenarios use estimations of reversed flux area growth from 1880 to 1990 CE (48).

ACKNOWLEDGMENTS. The work benefited from comments and suggestions by two anonymous reviewers, the associated editor, and a critical presubmission reading by E. Tohver. Jennifer Strehlau performed sample dissolution and extraction [University of Minnesota (UMN) Department of Chemistry]. We are grateful to Instituto Brasileiro do Meio Ambiente e dos Recursos Renováveis for permission to collect stalagmite samples. This work was supported by São Paulo Research Foundation Grants 2016/00299-4, 2016/24870-2, 2017/50085-3, 2018/07410-3, and 2016/15807-5; and Conselho Nacional de Desenvolvimento Científico e Tecnológico Grants 206997/2014-0 and 405179/2016-2. The study was financed in part by the Coordenação de Aperfeiçoamento de Pessoal de Nível Superior (Finance Code 001). P.J. acknowledges a National Science Foundation Visiting fellowship to IRM/UMN (IRM manuscript no. 1815). The use of specific trade names does not imply endorsement of products or companies by the National Institute of Standards and Technology but are used to fully describe the experimental procedures.

- 25. Dreybrodt W, Scholz D (2011) Climatic dependence of stable carbon and oxygen isotope signals recorded in speleothems: From soil water to speleothem calcite. Geochim Cosmochim Acta 75:734-752.
- 26. Novello VF, et al. (2016) Centennial-scale solar forcing of the South American monsoon system recorded in stalagmites. Sci Rep 6:24762.
- 27. Maxbauer DP, Feinberg JM, Fox DL (2016) MAX UnMix: A web application for unmixing magnetic coercivity distributions. Comput Geosci 95:140-145.
- 28. Egli R (2004) Characterization of individual rock magnetic components by analysis of remanence curves, 1. Unmixing natural sediments. Stud Geophys Geod 48:391-446.
- 29. Osete ML, et al. (2012) The Blake geomagnetic excursion recorded in a radiometrically dated speleothem. Earth Planet Sci Lett 353:173-181.
- 30. Font E, et al. (2014) Magnetic fingerprint of southern Portuguese speleothems and implications for paleomagnetism and environmental magnetism. J Geophys Res Solid Earth 119:7993-8020.
- 31. Zhu Z, et al. (2017) Holocene ENSO-related cyclic storms recorded by magnetic minerals in speleothems of central China. Proc Natl Acad Sci USA 114:852-857
- 32. Jaqueto P, et al. (2016) Linking speleothem and soil magnetism in the Pau d'Alho cave (central South America). J Geophys Res Solid Earth 121:7024-7039.
- 33. Bourne MD, et al. (2015) Long-term changes in precipitation recorded by magnetic minerals in speleothems. Geology 43:595-598.
- 34. Ponte JM, Font E, Veiga-Pires C, Hillaire-Marcel C, Ghaleb B (2017) The effect of speleothem surface slope on the remanent magnetic inclination. J Geophys Res Solid Earth 122:4143-4156.
- 35. Jackson MJ, Banerjee SK, Marvin JA, Lu R, Gruber W (1991) Detrital remanence, inclination errors, and anhysteretic remanence anisotropy-Quantitative model and experimental results. Geophys J Int 104:95-103.
- 36. Tauxe L, Pick T, Kok YS (1995) Relative paleointensity in sediments-A pseudo-Thellier approach. Geophys Res Lett 22:2885-2888.
- 37. Terra-Nova F, Amit H, Hartmann GA, Trindade RIF (2016) Using archaeomagnetic field models to constrain the physics of the core: Robustness and preferred locations of reversed flux patches. Geophys J Int 206:1890-1913.
- 38. Terra-Nova F, Amit H, Hartmann GA, Trindade RIF, Pinheiro KJ (2017) Relating the South Atlantic anomaly and geomagnetic flux patches. Phys Earth Planet Inter 266:39-53.
- 39. Cheng H, et al. (2013) Improvements in Th-230 dating, Th-230 and U-234 half-life values, and U-Th isotopic measurements by multi-collector inductively coupled plasma mass spectrometry. Earth Planet Sci Lett 371:82-91.
- 40. Scholz D, Hoffmann DL (2011) StalAge-An algorithm designed for construction of speleothem age models. Quat Geochronol 6:369-382.
- 41. Kirschvink JL (1980) The least-squares line and plane and the analysis of palaeomagnetic data. Geophys J Int 62:699-718.
- 42. Zhao X, Heslop D, Roberts AP (2015) A protocol for variable-resolution first-order reversal curve measurements. Geochem Geophys Geosyst 16:1364–1377.
- 43. Zhao X, et al. (2017) Magnetic domain state diagnosis using hysteresis reversal curves. J Geophys Res Solid Earth 122:4767–4789.
- 44. Strehlau JH, Hegner LA, Strauss BE, Feinberg JM, Penn RL (2014) Simple and efficient separation of magnetic minerals from speleothems and other carbonates. J Sediment Res 84:1096-1106.
- 45. Fisher R (1953) Dispersion on a sphere. Proc R Soc A 217:295-305.
- 46. Bullard EC, Freedman C, Gellman H, Nixon J (1950) The westward drift of the earth's magnetic field. Philos Trans R Soc A 243:67-92.
- 47. Olson P, Amit H (2006) Changes in earth's dipole. Naturwissenschaften 93:519-542. 48. Metman MC. Livermore PW. Mound JE (2018) The reversed and normal flux contri-
- butions to axial dipole decay for 1880-2015. Phys Earth Planet Inter 276:106-117.